Ultrasonics 93 (2019) 63–70

Contents lists available at ScienceDirect

Ultrasonics

journal homepage: www.elsevier.com/locate/ultras

# Ultrasound attenuation and phase velocity of moderately concentrated silica suspensions

Hayato Mori, Tomohisa Norisuye*, Hideyuki Nakanishi, Qui Tran-Cong-Miyata

*Department of Macromolecular Science and Engineering, Graduate School of Science & Technology, Kyoto Institute of Technology, Matsugasaki, Sakyo-ku, Kyoto 606-8585, Japan*

ARTICLE INFO

*Keywords:*
Attenuation
Sound velocity
Microparticle
Scattering

ABSTRACT

Ultrasound attenuation coefficient and phase velocity of moderately concentrated suspensions of charged silica particles were measured as a function of frequency. The attenuation coefficients were found to be significantly smaller than the theoretical prediction, and such a difference did not appear in the neutral particle suspensions under the corresponding concentrations. In this study, we have investigated the acoustic spectra of silica particles with different particle sizes, concentrations as well as salt concentrations. It was revealed that the noticeable deviation from the theoretical estimation only appeared in the case of large particle sizes close to the wavelength of ultrasound, and could be circumvented by addition of small amount of salt to suppress the electrostatic interactions of the charged silica particles.

## 1. Introduction

Ultrasonic spectroscopy (US) is a useful tool to determine the viscoelasticity of material in the ultrasound frequency range [1]. When microparticles are dispersed in liquid, the size and the elasticity of particle in the suspension can be quantitatively determined with an aid of the acoustic scattering theories [2,3]. Originally, Epstein and Carhart formulated the theory to reproduce the attenuation coefficient of liquid droplets [4]. Later, the theory was extended to the case of solid particles dispersed in liquid [5]. The theory was abbreviated as the ECAH theory by their contributions. The ECAH theory was generalized to either liquid or solid particles dispersed in a liquid or solid matrix by introducing "wild-card" variables. This allows us to convert the velocity potential of liquid to the displacement potential of solid, or vice-versa [6,7]. Compared to other classical theories given by Anderson [8] or by Faran [9], the ECAH theory takes contributions of both viscous and thermal waves into account. Although the parameters associated with the thermal waves make the analysis more complicated and ambiguous due to increase in the number of adjustable parameters, the effect becomes more important for nanoparticles, where the size of particle is comparable with the wavelength of thermal waves.

While nano-sized objects are matter of importance in the material science, particles in liquid often experience formation of unfavorable aggregates and/or agglomerates. Therefore, quantitative characterization of such aggregates typically in the micrometer range is also an important strategy to control the properties and functionality of the suspensions. So far, rigid microparticles of polystyrene and polydivinylbenzene (PDVB) were investigated in the range 0.5–10 wt% using two longitudinal ultrasound wave transducers operated at 2–40 MHz depending on the target particle size [10]. When the elastic particles with the sizes comparable to the wavelengths of ultrasound are dispersed in water, strong peaks in attenuation and phase velocity (or acoustic impedance) are observed due to the acoustic resonance [11–13]. In addition to particle sizing, the analysis of the elasticity and thickness of microcapsule could be carried out based on the ultrasound scattering analysis with the scattering function of core-shell structures [14].

For suspensions with a finite concentration, multiple scattering theories are employed. For example, independent scattering approach (ISA) is a useful model [15]. At relatively low concentrations, this formula is equivalent to the case of single scattering. This model is believed to be valid up to 20% for polystyrene particles, and up to 30% for emulsions [6]. As for more elaborate models, the multiple scattering theory proposed by Waterman-Truell [16] or Lloyd-Berry [17] is combined with the ECAH theory. Needless to say, these approaches have a limitation in terms of the applicable concentration because all these models utilize the ECAH single scattering function. As the particle concentration becomes larger, there exists an overlapping of the scattered waves due to the short inter-particle distance. As for the overlapping of the shear waves and the thermal waves, the coupled phase

* Corresponding author.
*E-mail address:* nori@kit.jp (T. Norisuye).

https://doi.org/10.1016/j.ultras.2018.10.010
Received 21 May 2018; Received in revised form 24 September 2018; Accepted 24 October 2018
Available online 31 October 2018
0041-624X/ 

model is a useful model [18,19]. At appreciable volume fraction, quasi-crystalline approximation (QCA) taking account of a higher order correction could be used [20,21].

As mentioned above, the data up to 20% could be reproduced by the acoustic scattering theories combining the ECAH single scattering theory and the dispersion relation. As a matter of fact, in our previous study, good agreement between the experimental results and the model was confirmed for the attenuation coefficient and the phase velocity of the PDVB particles [10]. Besides the success, those of moderately concentrated charged particles are not well investigated particularly for the micron-sized particles. In this study, measurements of the attenuation coefficient and the phase velocity of the silica particles having negative charges on the surface will be demonstrated. Finally, effects of the salt concentration and the particle size dependences on the acoustic properties will be described.

## 2. Experimental procedure

Monodisperse silica standard microspheres were purchased from Sekisui Chemical (JAPAN). Prescribed amount of the particles was dispersed in an aqueous solution to obtain the suspension with desired concentration $C$, followed by a brief immersion in a low power ultrasonic bath prior to ultrasound scattering experiments in order to avoid aggregation. Water was purified twice by filtering through a 0.2 μm membrane filter after distillation. Sodium chloride was purchased from Wako Chemical (JAPAN) and used without further purification. In this study, the dependence of the acoustic spectra on the salt concentration $C_s$ was examined. Since the aqueous suspension of the as-received sample may not be exactly salt-free, the effective salt concentration in distilled water was measured by conductivity measurements. As the results, the concentration was found to be 8.67 μM, which was sufficiently low compared to the salt concentrations studied here. The zeta potential in highly turbid suspension was acoustically determined and was approximately −90 mV obtained by an independent electrophoretic mobility experiment. The details will be shown in the forthcoming paper. Further dialysis was not performed because the properties in extremely low salt concentrations (regarded as a salt-free system) are not the scope of this work. Disposable polystyrene rectangular vessels with the dimension $10 \times 10 \times 40\,mm^3$ and the wall thickness 1 mm were used as the sample cells.

The experimental setup is schematically illustrated in Fig. 1. An ultrasound pulse was generated using a broadband pulser/receiver (JSR DPR500) with a high-frequency remote pulser RP-H4. Water-immersion longitudinal plane wave transducers having different nominal frequencies, such as KGK B20K2I (diameter 2 mm, 20 MHz) and KGK B30K1I (1 mm, 30 MHz), were employed to examine the frequency dependences of the phase velocity and attenuation coefficient of the materials.

The transmitted pulse was received by another transducer, followed by the amplification using the receiver. The sample cell and transducer were carefully aligned by a homemade stainless stage equipped with microstages (X, Y, Z, α, and β). The signal was recorded by a 12-bit high-speed digitizer, GaGe CS121G2, at a sampling rate of 1 Giga samples/s. The trigger timing was controlled by using a square pulse generated by an arbitrary wave generator (Keysight Technologies, 33521B). A digital delay (Stanford, DG645) was employed to control the acquisition timing of the input and output signals by taking account of the traveling time of sound in water. The digital equipment was synchronized with a 10 MHz reference clock to avoid phase jittering. The pulse repetition time was set at 0.5 ms and the pulse was averaged over 5000 times to achieve good precision. The sample was set in a homemade thermostat bath regulated at 25 ± 0.005 °C. The temperature stability was confirmed by measuring the stability of the phase velocity obtained over 6 digits for deuterated water using multi-echo reflection ultrasonic spectroscopy (MERUS) [22,23].

Field-emission SEM (FE-SEM; JEOL JSM-7600F) images were taken to verify the particle size and its distribution. The obtained bitmap images were recorded with 2560 × 1920 pixels containing about 10 particles in each picture, followed by the calculation of the diameter for at least 300 particles. The particle density was determined by the density matching method with calibrated aqueous solutions of sodium polytungstate, SPT ($3Na_2WO_4{\cdot}9WO_3{\cdot}H_2O$). The density of the SPT solution was calibrated using a 25 mL Gay-Lussac pycnometer prior to the density matching experiments. The sample name, the average diameter $d$ calibrated by SEM, the coefficient of variation CV (the standard deviation of particle diameter normalized by the $d$), and the density of particle ρ are summarized in Table 1.

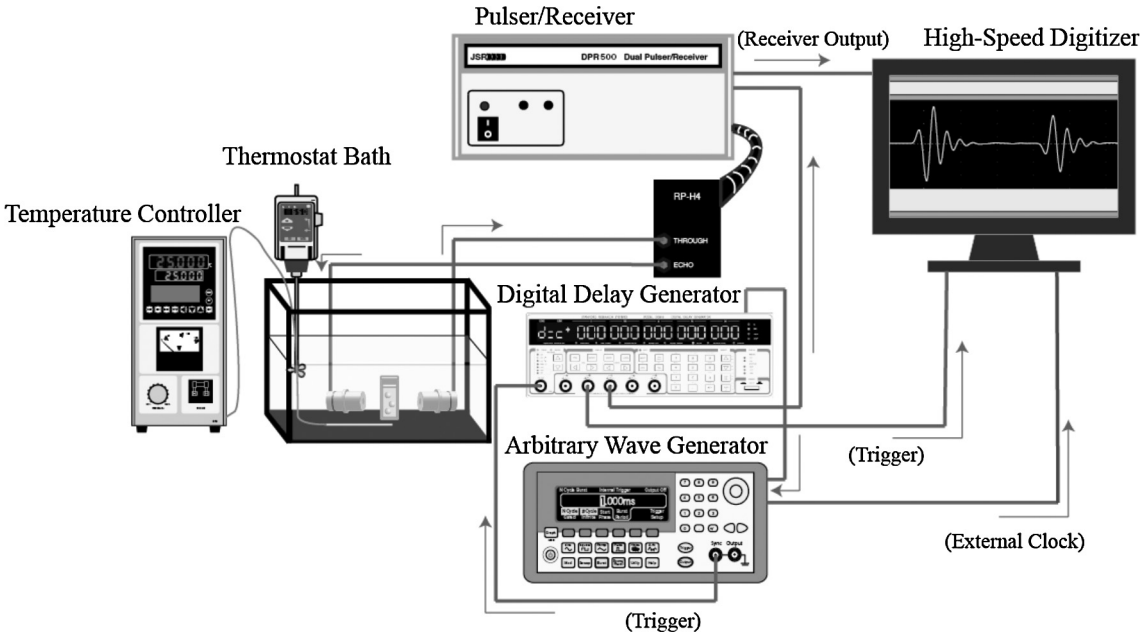


**Fig. 1.** Experimental setup of the ultrasonic spectroscopy method.

**Table 1**
The sample name, the average diameter $d$ calibrated by SEM, the coefficient of variation CV (the standard deviation of particle diameter normalized by the $d$), and the density of particle ρ.

| Sample | $d$ (μm) | CV | ρ (g/cm$^3$) |
|---|---|---|---|
| dS110 | 0.109 ± 0.011 | 0.110 | 1.85 ± 0.03 |
| dS555 | 0.555 ± 0.023 | 0.042 | 1.86 ± 0.03 |
| d3 | 2.83 ± 0.03 | 0.011 | 2.01 ± 0.015 |
| d5 | 4.63 ± 0.04 | 0.009 | 2.08 ± 0.010 |
| d7 | 6.68 ± 0.07 | 0.011 | 2.01 ± 0.015 |
| d10 | 9.91 ± 0.15 | 0.015 | 2.07 ± 0.015 |

## 3. Data analysis

The frequency $f$, dependence of the intensity attenuation coefficient, $\alpha$, and the velocity of ultrasound, $c$, were acquired by ultrasonic transmission spectroscopy [10,11,14,22–24]. They were analyzed using the following relations,

$$\alpha(f) = -\frac{2}{L}\left\{\ln\frac{A_{\mathrm{sam}}(f)}{A_{\mathrm{ref}}(f)}\right\} + \alpha_{\mathrm{ref}}(f) \tag{1}$$

$$c(f) = \frac{2\pi fL}{\theta_{\mathrm{sam}}(f) - \theta_{\mathrm{ref}}(f) + \frac{2\pi fL}{c_{\mathrm{ref}}(f)} + 2m\pi} \tag{2}$$

where $L$ is the sample size, $A$ is the amplitude and $\theta$ is the phase of the transmitted pulse, and the subscript "0", "sam" and "ref" respectively refer to the incident pulse and the transmitted pulse for the sample and reference. Evaluation of the appropriate number of $m$, is described elsewhere [22]. The transmission loss due to mismatch of the acoustic impedance between the sample and the cell wall is negligibly small in our case. The intensity attenuation, $\alpha_{\mathrm{ref}}/f^2$ and the sound speed in distilled water, $c_{\mathrm{ref}}$, employed as a known reference were respectively 1496.7 (m/s) and $4.38 \times 10^{-14}$ (S$^2$/m) [25,26]. $L$ was precisely calibrated by a pulse echo measurement, and the typical value of $L$ was approximately 10 mm.

The theoretical values of $\alpha$ and $c$ for particle suspensions were calculated using the real and imaginary part of the effective wavenumber $k$ given by,

$$k = \frac{2\pi f}{c} + \mathrm{i}\frac{\alpha}{2} \tag{3}$$

The single particle scattering function $F(\Theta)$ at the angle $\Theta$, and the wavenumber $k$ are correlated by the dispersion relation [15–17,27]. In this study, the Lloyd-Berry equation [17],

$$\left(\frac{k}{k_0}\right)^2 = 1 + \sum_j \left\{\frac{4\pi N_j(d_j)F_j(0)}{k_0^2} - \frac{4\pi^2 N_j^2(d_j)}{k_0^4}\left[F^2(0) - F^2(\pi) + \int_0^\pi \frac{1}{\sin(\Theta/2)}\frac{\mathrm{d}}{\mathrm{d}\Theta}F^2(\Theta)\mathrm{d}\Theta\right]\right\} \tag{4}$$

and the Waterman-Truell equation [16],

$$\left(\frac{k}{k_0}\right)^2 = 1 + \sum_j \left\{\frac{4\pi N_j(d_j)F_j(0)}{k_0^2} + \frac{4\pi^2 N_j^2(d_j)}{k_0^4}[F^2(0) - F^2(\pi)]\right\} \tag{5}$$

were employed to reproduce the acoustic properties at finite concentrations where $N_j(d_j)$ is the number concentration of particle with the diameter $d_j$ for the $j$th particle, $k_0$ is the complex wavenumber for the reference given by,

$$k_0 = \frac{2\pi f}{c_{\mathrm{ref}}} + \mathrm{i}\frac{\alpha_{\mathrm{ref}}}{2} \tag{6}$$

$F(\Theta)$ is the scattering function given by,

$$F(\Theta) = \frac{1}{\mathrm{i}k_0}\sum_{n=0}^{\infty}(2n+1)A_nP_n(\cos\Theta) \tag{7}$$

where $P_n$ is the Legendre polynomials of the $n$th order, and $A_n$ is the scattering amplitude [10]. The partial wave amplitude of the micron-sized particle in viscous fluid was derived previously and solved by the wave equations in terms of the radial and tangential pressure and those of displacement. Hereafter, the model is abbreviated as ECAH44. While the viscous waves are taken into account, the thermal contribution could be negligibly small for our silica particles studied here. Then, the estimated scattering amplitude is substituted into the dispersion relation, Eqs. (4) or (5) to evaluate the attenuation coefficient and velocity of ultrasound.

## 4. Results and discussions

Fig. 2(a) shows the attenuation coefficient $\alpha$ and the phase velocity $c$ as a function of frequency obtained for d10 at the particle concentration, $C = 0.3$ wt%. The experimental results obtained by the 30 MHz transducer were reproduced by the ECAH44 model with the dispersion relation as indicated by the solid lines. All the parameters required to reproduce the results are summarized in Table 2, and will be discussed

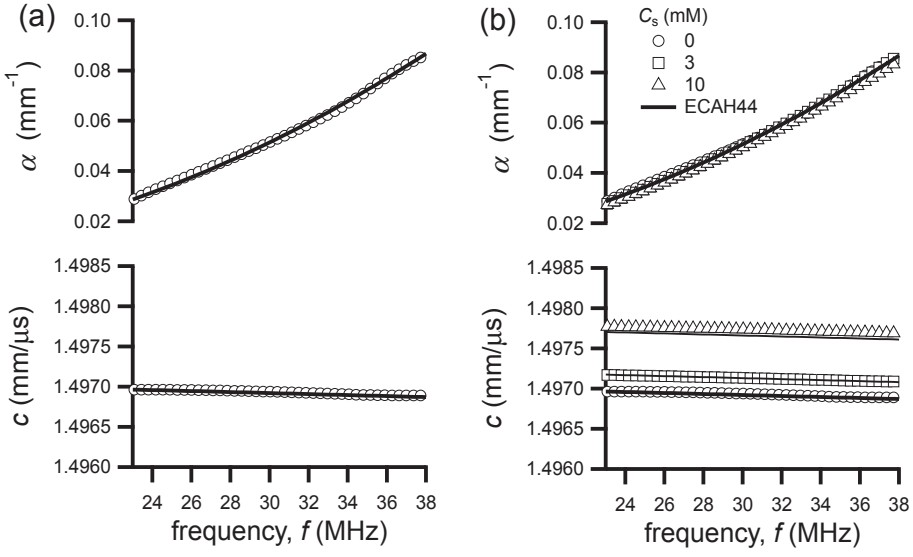


**Fig. 2.** The frequency dependences of $\alpha$ and $c$ obtained for d10 at 0.3 wt% without NaCl (a) with NaCl (b).

**Table 2**
Parameters used in the US calculation.

| Sample | ρ (g/cm$^3$) | $c_L$ (mm/μs) | $c_S$ (mm/μs) | $E$ (GPa) | $G$ (GPa) | $K$ (GPa) | $\sigma$ |
|---|---|---|---|---|---|---|---|
| Fused silica [6] | 2.185 | 5.968 | 3.761 | 72.35 | 30.90 | 36.62 | 0.170 |
| d3 | 2.01 | 5.5 | 3.2 | 51.21 | 20.58 | 33.36 | 0.244 |
| d5 | 2.08 | 5.5 | 3.3 | 55.21 | 22.65 | 32.72 | 0.219 |
| d7 | 2.01 | 5.5 | 3.2 | 51.21 | 20.58 | 33.36 | 0.244 |
| d10 | 2.07 | 5.5 | 3.3 | 54.95 | 54.95 | 32.56 | 0.219 |
| Borosilicate glass [28] | 2.069 | 4.534 | 2.628 | 35.65 | 14.29 | 23.47 | 0.259 |

later. $c_L$, $c_S$, $E$, $G$, $K$, and $\sigma$ are respectively the longitudinal velocity, shear velocity, Young's modulus, shear modulus, bulk modulus and the Poisson's ratio of the particle. Since the concentration is sufficiently low, the results calculated by the dispersion relations given by Waterman-Truell and Lloyd-Berry were identical. At this low concentration regime, there is no anomaly in the interpretation of the attenuation data.

Fig. 2(b) shows the results similar to Figure (a) except the presence of salt. As shown in the figure, the attenuation coefficient was almost identical to all the salt concentrations. On other hand, the phase velocity systematically increased with the salt concentration. Increase in $c$ is due to the presence of salt contributing to the effective velocity. Therefore, with appropriate background data of the surrounding liquid consisting of water and salt, all the phase velocities were successfully reproduced by the scattering theory (fitted lines were not shown for the clarity of presentation). It is noted again that there is no anomaly in the interpretation of the acoustical data at this low concentration regime.

Fig. 3 shows the frequency dependence of the $\alpha$ and $c$ obtained for d10 with $C$ = 10 wt%. Although the validity of the ECAH analysis was confirmed up to the particle volume fraction of 20%, the experimental data was significantly smaller than the theoretical prediction beyond the experimental error. The dashed lines are the results calculated based on the parameters for the fused silica reported in the literature

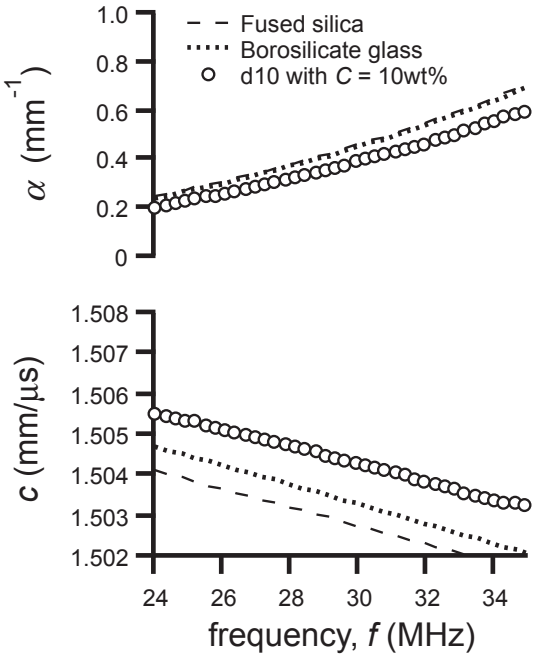


**Fig. 3.** The frequency dependences of $\alpha$ and $c$ obtained for d10 at 10 wt% without NaCl. The data could not be reproduced by the present scattering function theories with given parameters.

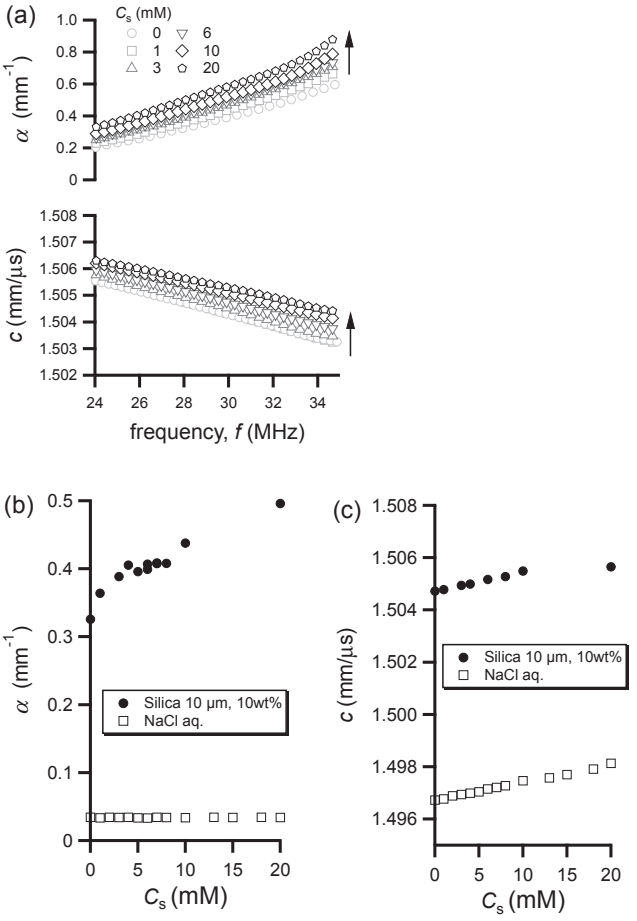


**Fig. 4.** (a) The frequency dependences of $\alpha$ and $c$ obtained for d10 with different $C_s$. (b) $C_s$ dependences of $\alpha$ and (c) $c$ extracted at 28 MHz.

[6]. Calculation based on the values for borosilicate glasses is also demonstrated [14,28]. Among various considerations, no appropriate parameter could be found to reproduce the data.

Before discussing the deviation of the calculation from the experimental results, let us show the way to successfully reproduce the data by the present scattering function analysis with given particle size distribution and the elasticity of the particles.

First of all, the attenuation coefficent obtained for d10 with $C$ = 10 wt% was found to be sensitive to the concentration of salt. As shown in Fig. 4(a), the frequency dependence of $\alpha$ systematically increased with the salt concentration, $C_s$. In order to clearly demonstrate the variation of $\alpha$ with $C_s$, $\alpha$ was extracted at 28 MHz and plotted as a function of $C_s$ in Fig. 4(b). It was found that $\alpha$ increased with $C_s$, and tends to level-off at high $C_s$. With increasing $C_s$, $\alpha$ increased again for $C_s$ > 10 mM presumably due to formation of large aggregates. Note that the attenuation coefficient of the NaCl solution without any particles was almost constant as shown by the open squares in Fig. 4(b).

Therefore, the increase in $\alpha$ of d10 with $C$ = 10 wt% (Fig. 3) is a unique characteristics found for the charge silica at the moderate concentration. As shown in Fig. 4(c), systematic increase in $c$ was observed for d10 with $C$ = 10 wt%. However, this behavior could be simply attributed to the effect of salt because $c$ obtained for the NaCl solution without particles increased with $C_S$ in the same slope. Therefore, analysis will be performed only for the behavior of attenuation coefficient in the following discussion.

Subsequently, the plateau regime of $C_s$ = 5–10 mM of $\alpha$ was explored more from different viewpoints. Fig. 5 shows the sedimentation velocity fluctuations, $\Delta V_y$ obtained by the dynamic ultrasound scattering (DSS) method, which allow us to evaluate the dynamics of

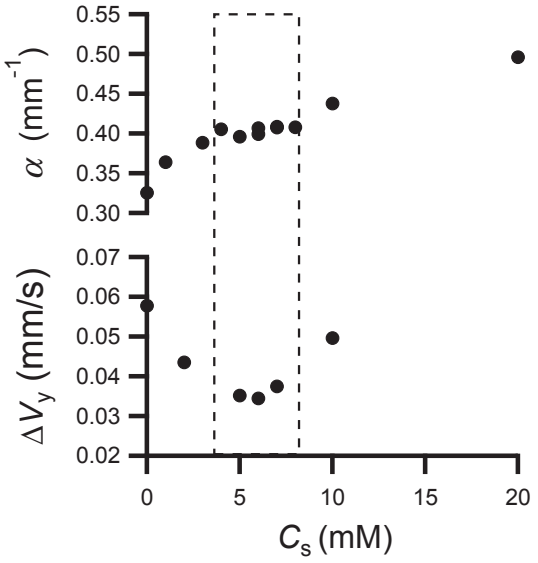


**Fig. 5.** $C_s$ concentration dependences of $\alpha$ and $\Delta V_y$ obtained for d10.

microparticles in highly turbid suspension [29–32]. $\alpha$ is also plotted together in the upper part of the figure in order to compare the data with $\Delta V_y$. The DSS experiments were performed by the same geometry with the US setup. When the micron-sized particles are dispersed in an aqueous solution, the particles settle down due to gravity. Due to long-ranged hydrodynamic interactions, the velocity field is not uniform, thereby showing fluctuations in the velocity [33–35]. When the dynamics is investigated along the sedimentation direction, z, the average sedimentation velocity $\langle V_z \rangle$ as well as its standard deviation $\Delta V_z$ could be evaluated. On the other hand, since the beam direction, y, is perpendicular to sedimentation ($\langle V_y \rangle = 0$), the standard deviation of the sedimentation velocity along the beam axis $\Delta V_y$ could be solely obtained. Note that the origin of the fluctuation is different from that of Brownian motion attributed to the thermal fluctuations of small particles. In our previous study [36], we showed that two important effects of salt on the dynamics of the charged particle suspensions existed: one was suppression of the electrostatic interactions of particle competing with the hydrodynamic interactions, and the other was particle aggregation due to the salting-out effects. Therefore, addition of large amount of salt could lead to an abrupt increase in the scattered intensity above $C_s = 7$ mM. The variation of the velocity fluctuations was explained by a model considering cooperative nature of the particles due to the long-ranged hydrodynamic interactions in terms of the

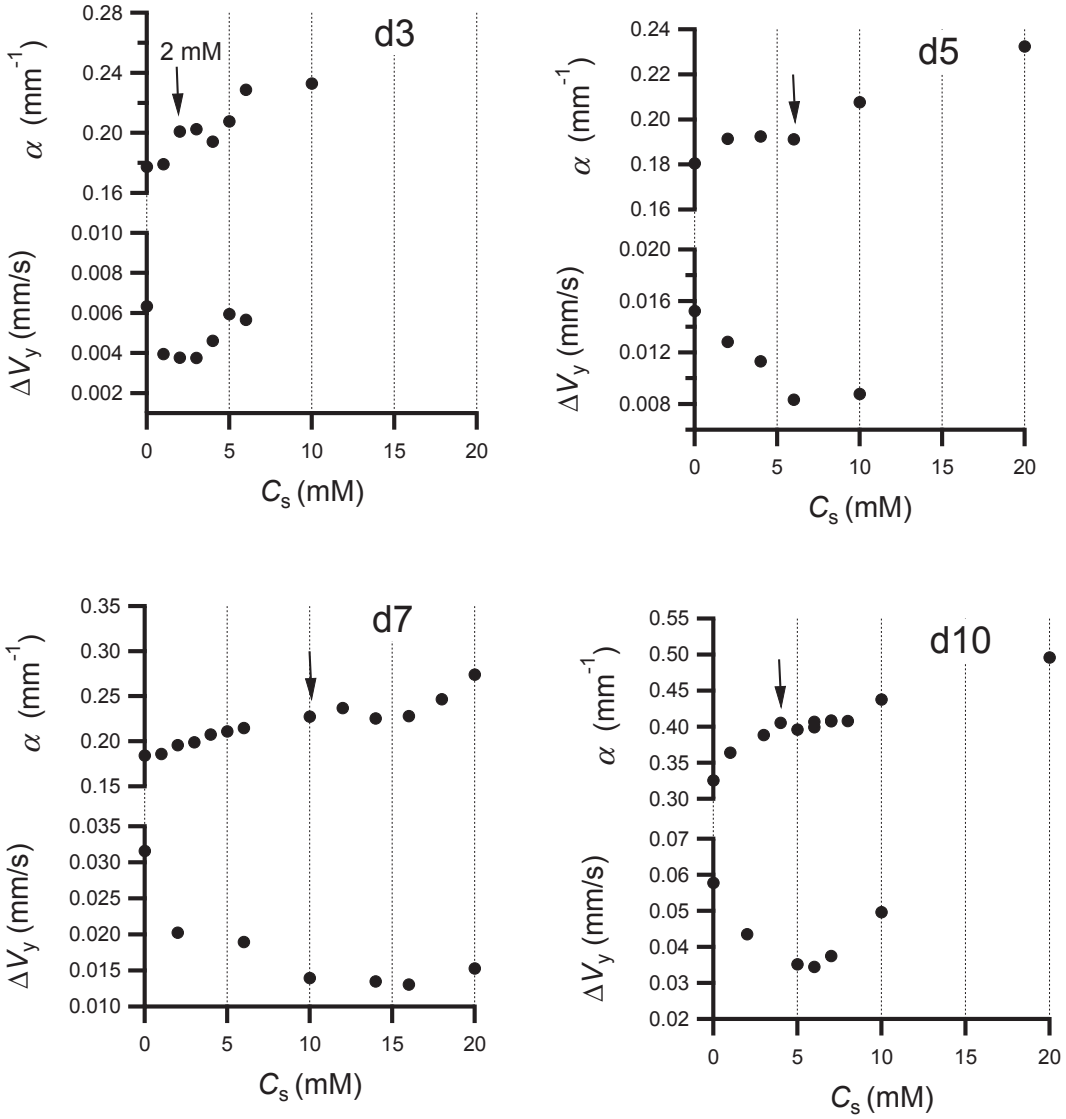


**Fig. 6.** The salt concentration dependences of $\alpha$ and $\Delta V_y$ obtained for the silica particle suspensions with the diameters d3, d5, d7 and d10.

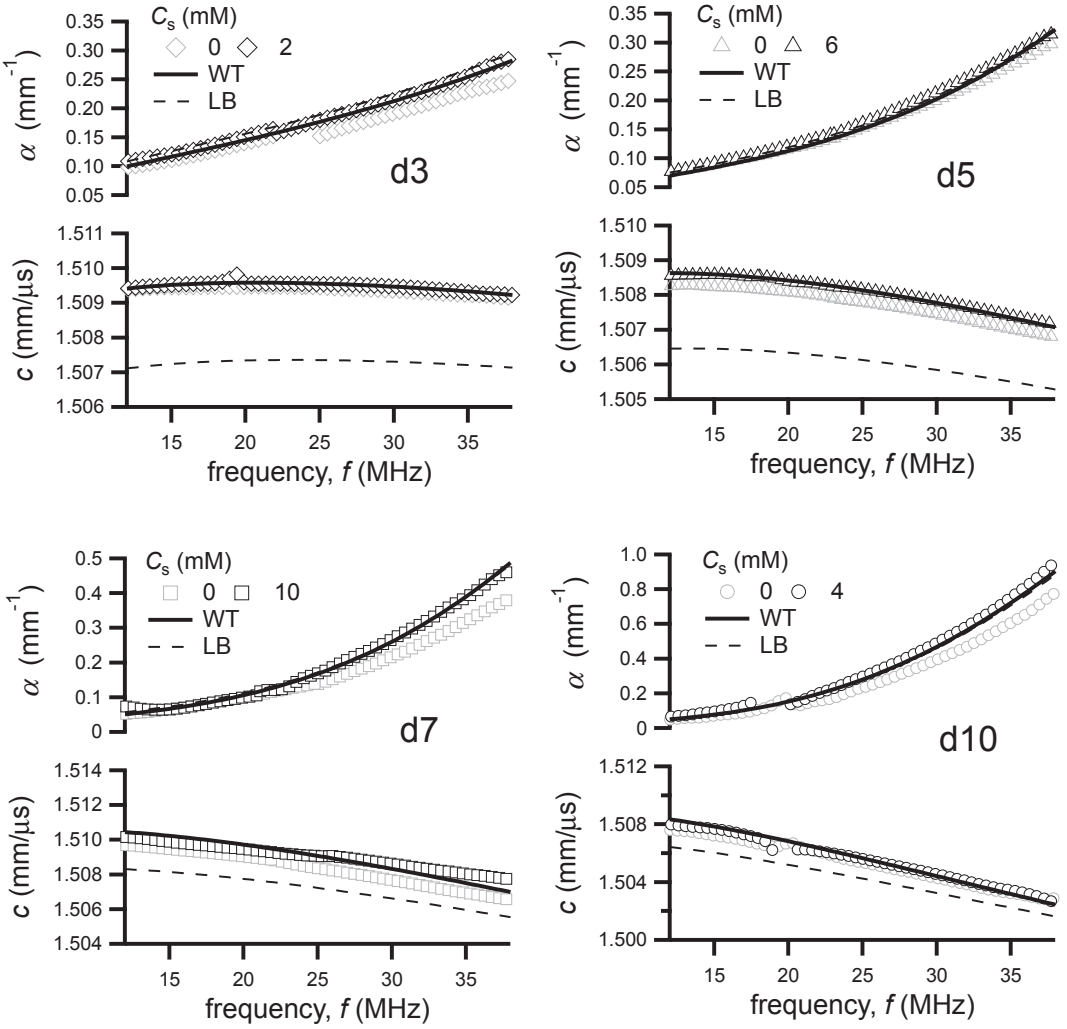


**Fig. 7.** The frequency dependences of $\alpha$ and $c$ obtained for the silica particle suspensions with $d$ = 3, 5, 7, 10 μm.

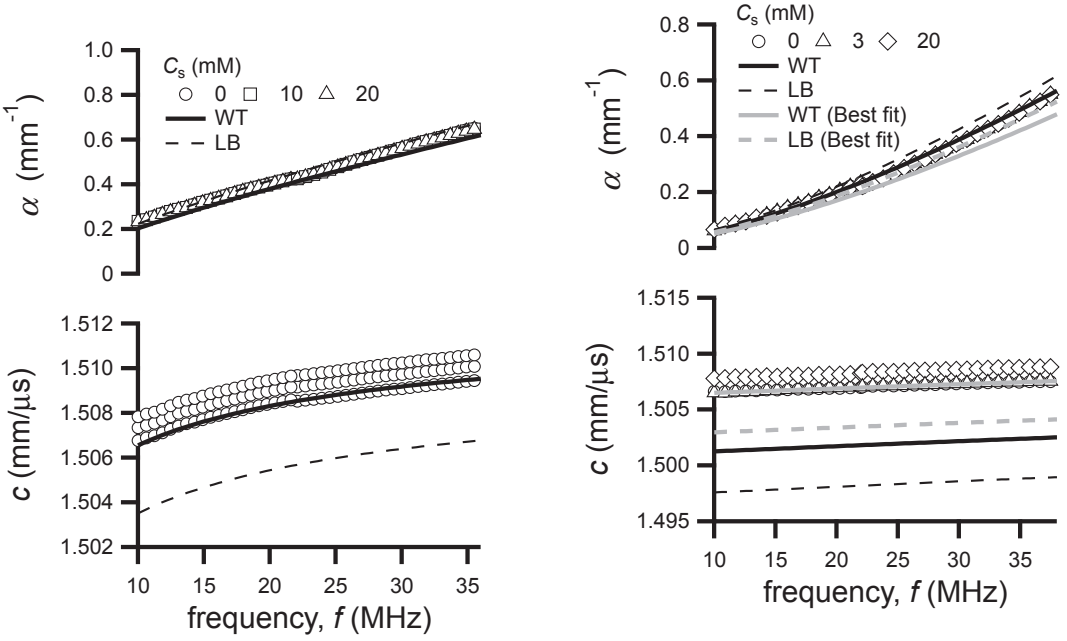


**Fig. 8.** The frequency dependences of $\alpha$ and $c$ obtained for (a) dS555 and (b) dS110.

**Table 3**
Parameters used in the US calculation.

| Sample | ρ (g/cm$^3$) | $c_L$ (mm/μs) | $c_S$ (mm/μs) | $E$ (GPa) | $G$ (GPa) | $K$ (GPa) | $\sigma$ |
|---|---|---|---|---|---|---|---|
| dS110 | 1.85 | 4.8 | 2.63 | 33.08 | 12.87 | 25.70 | 0.285 |
| dS555 | 1.86 | 4.8 | 2.63 | 33.08 | 12.87 | 25.70 | 0.285 |

dependence on the particle size, volume fraction, and correlation length [33–35]. While anomalous volume fraction dependence appeared when charged particles are examined, addition of salt suppressed the anomalous increase in the velocity fluctuation, and then $\Delta V_y$ followed the conventional hydrodynamic model, as expected. Therefore, the minimum in $\Delta V_y$ could be a measure for ideal conditions of particles. Below the salt concentration, the strong electrostatic interactions are present in the system and therefore particles could be stably dispersed in the suspension. Particularly, above this salt concentration, repulsive electrostatic interactions are screened out to have a weak particle association. The plateau of $\alpha$ coincided with the minimum of $\Delta V_y$ as shown in Fig. 5. This suggests that it could be an ideal (random) particle structure, which is relevant to be analyzed using the scattering function theory with the dispersion relation assuming the random structure of particles.

Fig. 6 summarizes the $C_s$ dependence of $\alpha$ and $\Delta V_y$ with different particle sizes. As seen from the figure, the plateau region of $\alpha$ was observed for all the silica particle sizes studied here. The specific salt concentrations, $C_s^*$, showing the minimum of $\Delta V_y$ were indicated by the arrows. For d3, d5 and d7, the plateau region shifted to the lower $C_s$ with decreasing the particle size. Therefore, for nanoparticles, it is expected that there is no anomaly in the attenuation coefficient. As a matter of fact, the excellent analysis on the silica nanoparticles using the present acoustic scattering theories was reported in the literature, where breakdown of the acoustic scattering model or description in terms of the addition of salt was not found [6]. Therefore, such a deviation of the attenuation data from the theoretical model could be the unique characteristics for the charged particle with the large particle size comparable with the wavelength of ultrasound and at moderately high concentration of particles.

Since it is expected that the strong repulsive interaction could be reasonably eliminated by addition of salt at the concentration $C_s^*$, theoretical reproduction of the experimental data using the present acoustic scattering theories of ECAH44 with the dispersion relation was attempted. As shown in Fig. 7, the attenuation coefficients obtained for d3, d5, d7, and d10 were successfully reproduced by the acoustic scattering theories. In order to ensure the discussion, the measurements were carried out using two-pairs (emitting and receiving) of broadband transducers (20 and 30 MHz) covering the broader frequency range from 10 to 40 MHz. The parameters employed in the analysis were summarized in Table 2. The experimental data were satisfactory agreed with the intermediate values of the longitudinal and shear velocities between those of fused silica and borosilicate glass reported in the literatures. As realized from the values of density, the evaluated longitudinal and shear velocities for our particle could be reasonable. The fixed value of the longitudinal velocity for the silica particle was employed throughout the analysis and the evaluated shear velocities for the silica particle were almost the same for all the particle sizes.

While the calculated attenuation coefficients were insensitive to the dispersion relations, reproduction of the phase velocity using Waterman-Truell model [16,27] was better than the Lloyd-Berry model. Although an error has already been pointed out by Lloyd and berry [17], experiments showed better agreement using the former equations in terms of the phase velocity.

In order to investigate the effect of salt on $\alpha$ and $c$ for silica particle with smaller particle sizes in the nanometers, silica particles are synthesized by hydrolysis and condensation of tetraalkoxide with ammonia, the so-called Stöber method. The particle diameter and the density were listed in Table 1.

Fig. 8 shows the frequency dependence of $\alpha$ and $c$ obtained for silica particles prepared by the Stöber method, dS110 and dS555 with $C$ = 10 wt%. For dS110 and dS555, it was found that the frequency spectra of $\alpha$ were almost overlapped with others obtained for the different salt concentrations. Similar to the results indicated in Fig. 4, the phase velocity systematically increased with the salt concentration. However, this increase was, as mentioned above, originated from the amount of salt present in the suspension. It is worth to recall that the results obtained for d10 show the noticeable salt effect, in the nanometers region and the data was insensitive to addition of salt. Since dS110 and dS555 are not standard particles but the synthesized particles having smaller densities, the expected longitudinal velocity of particle could be smaller than those of d3, d5, d7 and d10. The best-fit parameters to reproduce the experimental curves are listed in Table 3. The evaluated longitudinal and shear velocity were close to the values of borosilicate glass.

The solid lines and dashed lines respectively correspond to the calculated curves using Waterman-Truell and Lloyd-Berry equations. Note that although the expected particle diameter $d$ and the density ρ were respectively 110 nm and 1.85 g/cm$^3$, the best-fit parameters were $d$ = 114 nm and ρ = 1.73 g/cm$^3$. This difference could be attributed to the fact that the calibration of the particle by an electron microscope and by weighing were performed after drying, not in-situ. These results are represented by the black and gray lines in the figure. Since the dispersion relation assumes that the particle positions are statistically random, a great care must be taken to completely reproduce the experimental data by the theory. This could be performed by taking a structure factor into account, but this requires independent experiments to determine the radial distribution function of the sample. Therefore, it is suggested to add a small amount of salt to screen out the electrostatic interaction as has been carried out in the traditional analysis of polymer electrolyte solutions.

## 5. Conclusions

The frequency dependences of the attenuation coefficient and the phase velocity obtained for the silica particles in aqueous suspension at moderately high concentrations were studied by ultrasonic spectroscopy (US). The US results revealed that the attenuation spectra obtained for the micron-sized particles exhibited significantly smaller values than those expected from the acoustic scattering theory. In this study, we employed the single particle scattering theory proposed by Epstein-Carhart-Allegra-Hawley with the dispersion relation given by Waterman-Truell and Lloyd-Berry. As long as the concentration is not too high, e.g. 20% of suspension, the experimental results would be reproduced by the scattering analysis. As a matter of fact, for nanoparticles, good agreements between the experiments and the theories have been reported. Since the micron-sized particles were the matter of our particular interest, when the US analysis was carried out with megahertz ultrasound, the interparticle distance in our suspension could be on the same order with the wavelength of ultrasound. Therefore, it is suggested that the structure factor (or pair-correlation function) could be incorporated in the dispersion relation to achieve the better agreement between the experiment and calculation. Since the calculation is complicated in terms of the effective amount of charge, as a tentative solution, we have instead shown that, addition of salt could be useful to perform equivalent acoustic scattering analysis based on the random structure. Last but not least, it is noted that such a consideration must be unnecessary for nanoparticles as reported in the literatures.

## Acknowledgements

This work was supported by KAKENHI (Grant-in-Aid for Scientific

Research), No. 15K05627 from the Ministry of Education, Science, Sports, Culture, and Technology. The authors wish to thank Mr. Kohsuke Takeda and Mr. Takehisa Inoue to assist preparation of some of the figures.

## References

[1] M.J.W. Povey, Ultrasonic Techniques for Fluids Characterization, Academic Press, San Diego, CA, 1997.
[2] R.E. Challis, A.K. Holmes, J.S. Tebbutt, R.P. Cocker, Scattering of ultrasonic compression waves by particulate filler in a cured epoxy continuum, J. Acoust. Soc. Am. 103 (1998) 1413–1420.
[3] R.E. Challis, V.J. Pinfield, Ultrasonic wave propagation in concentrated slurries – the modelling problem, Ultrasonics 54 (2014) 1737–1744.
[4] P. Epstein, R.R. Carhart, The absorption of sound in suspensions and emulsions. I. Water fog in air, J. Acoust. Soc. Am. 25 (1953) 553–565.
[5] J.R. Allegra, S.A. Hawley, Attenuation of sound in suspensions and emulsions: theory and experiments, J. Acoust. Soc. Am. 51 (1972) 1545–1564.
[6] R.E. Challis, M.J.W. Povey, M.L. Mather, A.K. Holmes, Ultrasound techniques for characterizing colloidal dispersions, Rep. Prog. Phys. 68 (2005) 1541–1637.
[7] R.E. Challis, J.S. Tebbutt, A.K. Holmes, Equivalence between three scattering formulations for ultrasonic wave propagation in particulate mixtures, J. Phys. D-Appl. Phys. 31 (1998) 3481–3497.
[8] V.C. Anderson, Sound scattering from a fluid sphere, J. Acoust. Soc. Am. 22 (1950) 426–431.
[9] J.J. Faran, Sound scattering by solid cylinders and spheres, J. Acoust. Soc. Am. 23 (1951) 405–418.
[10] H. Mori, T. Norisuye, H. Nakanishi, Q. Tran-Cong-Miyata, Ultrasound attenuation and phase velocity of micrometer-sized particle suspensions with viscous and thermal losses, Ultrasonics 83 (2018) 171–178.
[11] K. Kubo, T. Norisuye, T.N. Tran, D. Shibata, H. Nakanishi, Q. Tran-Cong-Miyata, Sound velocity and attenuation coefficient of hard and hollow microparticle suspensions observed by ultrasound spectroscopy, Ultrasonics 62 (2015) 186–194.
[12] G.C. Gaunaurd, W. Wertman, Comparison of effective medium theories for inhomogeneous continua, J. Acoust. Soc. Am. 85 (1989) 541–554.
[13] X. Ji, M. Su, J. Chen, X. Wang, X. Cai, A novel method for plastic particle sizing in suspension based on acoustic impedance spectrum, Ultrasonics 77 (2017) 224–230.
[14] T.N. Tran, T. Norisuye, D. Shibata, H. Nakanishi, Q. Tran-Cong-Miyata, Determination of particle size distribution and elastic properties of silica microcapsules by ultrasound spectroscopy, Jpn. J. Appl. Phys. 55 (2016) 07KC01.
[15] L.L. Foldy, The multiple scattering of waves. I. General theory of isotropic scattering by randomly distributed scatterers, Phys. Rev. 67 (1945) 107–119.
[16] P.C. Waterman, R. Truell, Multiple scattering of waves, J. Math. Phys. (NY) 2 (1961) 512–537.
[17] P. Lloyd, M.V. Berry, Wave propagation through an assembly of spheres Iv. Relations between different multiple scattering theories, Proc. Phys. Soc. 91 (1967) 678–688.
[18] J.M. Evans, K. Attenborough, Coupled phase theory for sound propagation in emulsions, J. Acoust. Soc. Am. 102 (1997) 278–282.
[19] J.M. Evans, K. Attenborough, Sound propagation in concentrated emulsions: comparison of coupled phase model and core-shell model, J. Acoust. Soc. Am. 112 (2002) 1911–1917.
[20] L. Tsang, J.A. Kong, H. Habashy, Multiple scattering of acoustic waves by random distribution of discrete spherical scatterers with the quasicrystalline and Percus-Yevick approximation, J. Acoust. Soc. Am. 71 (1982) 552–558.
[21] H. Yang, W. Seong, K. Lee, Model-data comparison of high frequency compressional wave attenuation in water-saturated granular medium with bimodal grain size distribution, Ultrasonics 82 (2018) 161–170.
[22] T. Norisuye, S. Sasa, K. Takeda, M. Kohyama, Q. Tran-Cong-Miyata, Simultaneous evaluation of ultrasound velocity, attenuation and density of polymer solutions observed by multi-echo ultrasound spectroscopy, Ultrasonics 51 (2011) 215–222.
[23] K. Takeda, T. Norisuye, Q. Tran-Cong-Miyata, Origin of the anomalous decrease in the apparent density of polymer gels observed by multi-echo reflection ultrasound spectroscopy, Ultrasonics 53 (2013) 973–978.
[24] T. Inoue, T. Norisuye, K. Sugita, H. Nakanishi, Q. Tran-Cong-Miyata, Size distribution and elastic properties of thermo-responsive polymer gel micro-particles in suspension probed by ultrasonic spectroscopy, Ultrasonics 82 (2018) 31–38.
[25] W. Marczak, Water as a standard in the measurements of speed of sound in liquids, J. Acoust. Soc. Am. 102 (1997) 2776–2779.
[26] J.M.M. Pinkerton, A pulse method for the measurement of ultrasonic absorption in liquids_results for water, Nature 26 (1947) 128–129.
[27] J.G. Fikioris, P.C. Waterman, Multiple scattering of waves. II. “Hole Corrections” in the scalar case, J. Math. Phys. (NY) 5 (1964) 1413–1420.
[28] L. Abd El-Latif, Ultrasonic study on the role of $Na_2O$ on the structure of $Na_2O$-$B_2O_3$ and $Na_2O$-$B_2O_3$-$SiO_2$ glasses, J. Pure Appl. Ultrason. 27 (2005) 80–91.
[29] K. Kobayashi, T. Norisuye, K. Sugita, H. Nakanishi, Q. Tran-Cong-Miyata, Dynamics of nanometer- and micrometer-sized particles in suspension probed by dynamic ultrasound scattering techniques, J. Appl. Phys. 122 (045106) (2017) 045108.
[30] T. Norisuye, Structures and dynamics of microparticles in suspension studied using ultrasound scattering techniques, Polym. Int. 66 (2017) 175–186.
[31] M.L. Cowan, J.H. Page, T. Norisuye, D.A. Weitz, Dynamic sound scattering: field fluctuation spectroscopy with singly scattered ultrasound in the near and far fields, J. Acoust. Soc. Am. 140 (2016) 1992–2001.
[32] M.L. Cowan, J.H. Page, D.A. Weitz, Velocity fluctuations in fluidized suspensions probed by ultrasonic correlation spectroscopy, Phys. Rev. Lett. 85 (2000) 453–456.
[33] P.N. Segrè, E. Herbolzheimer, P.M. Chaikin, Long-range correlations in sedimentation, Phys. Rev. Lett. 79 (1997) 2574–2577.
[34] É. Guazzelli, J. Hinch, Fluctuations and instability in sedimentation, Annu. Rev. Fluid Mech. 43 (2011) 97–116.
[35] É. Guazzelli, J.F. Morris, A Physical Introduction to Suspension Dynamics, Cambrige, NY, 2012.
[36] K. Sugita, T. Norisuye, H. Nakanishi, Q. Tran-Cong-Miyata, Effect of electrostatic interactions on the velocity fluctuations of settling microspheres, Phys. Fluids 27 (2015) 013304.